Electronic Supplementary Material (ESI) for Physical Chemistry Chemical Physics.

Supporting Information:

Mesoscopic simulations of the in situ NMR spectra of porous carbon based supercapacitors: Electronic structure and adsorbent reorganisation effects

Anagha Sasikumar,[†,‡] Anouar Belhboub,[†,‡,¶] Camille Bacon,[§,‖] Alexander C. Forse,[⊥] John M. Griffin,[#] Clare P. Grey,[⊥] Patrice Simon,[†,‡] and Céline Merlet[*,†,‡]

†*CIRIMAT, Université de Toulouse, CNRS, Bât. CIRIMAT, 118, route de Narbonne 31062 Toulouse cedex 9, France*

‡*Réseau sur le Stockage Électrochimique de l'Énergie (RS2E), Fédération de Recherche CNRS 3459, HUB de l'Énergie, Rue Baudelocque, 80039 Amiens, France*

¶*École Centrale Casablanca, Ville verte, Bouskoura, 27182, Casablanca, Morocco*

§*Sorbonne Université, CNRS, Physico-Chimie des Électrolytes et Nanosystèmes Interfaciaux, F-75005 Paris, France*

‖*Maison de la Simulation CEA, CNRS, Université Paris-Sud, UVSQ, Université Paris-Saclay, F-91191 Gif-sur-Yvette, France*

⊥*Department of Chemistry, University of Cambridge, Lensfield Road, Cambridge, CB2 1EW, UK*

#*Department of Chemistry, Lancaster University, Lancaster, LA1 4YB, UK*

E-mail: merlet@chimie.ups-tlse.fr

1 Details of the molecular dynamics simulations for the calculation of free energy profiles

Molecular dynamics simulations are performed to obtain free energy profiles for the species considered in the NMR spectra calculation. For [BMI][BF_4]-ACN, the ions and solvent are represented using a coarse grained approach where three sites are used for cations and acetonitrile molecules and one site for anions. For the other electrolytes, an all-atom model is used. The intermolecular forces are calculated by the sum of Lennard-Jones and electrostatic interactions. Parameters of the force field can be found in published works[S1–S6] except for the Lennard-Jones parameters of the carbon in the case of [EMI][TFSI] which were taken equal to $\sigma = 3.34$ Å and $\varepsilon = 0.51$ kJ mol $^{-1}$. The model supercapacitors consist in slit pores with two electrodes of three graphene sheets each. All simulations are conducted in the NVT ensemble at 298K. Two-dimensional periodic boundary conditions are adopted to avoid unrealistic interactions between the electrodes. A timestep of 1 fs (respectively 2 fs) is used to integrate the equations of motion for all-atom simulations (respectively coarse-grained simulations). Simulations were performed at various potential differences applied between the electrodes with a constant potential method[S7–S9] using the LAMMPS or MetalWalls software.[S10,S11] Most of the initial configurations were generated using fftool.[S12] The systems are equilibrated for several nanoseconds until the electrode charge reaches a plateau before collecting data for several nanoseconds to calculate the free energies. Details of compositions and simulation box sizes of the considered systems are given in Table S1.

Table S1: Details of the simulated boxes for the various electrolytes studied in this work.

System	No. of ion pairs	No. of ACN	L_x (Å)	L_y (Å)	L_z (Å)
[BMI][BF_4]-ACN	96	896	32.24	34.36	118.90
[PEt_4][BF_4]-ACN	65	600	32.24	34.36	84.26
[EMI][TFSI]	322	–	34.08	36.89	146.05

2 Free energy profiles

Figure S1 shows the free energy profiles for BF_4^- in [BMI][BF_4]-ACN at the negative electrode. The desorption of anions at the negative electrode for non-zero potential differences

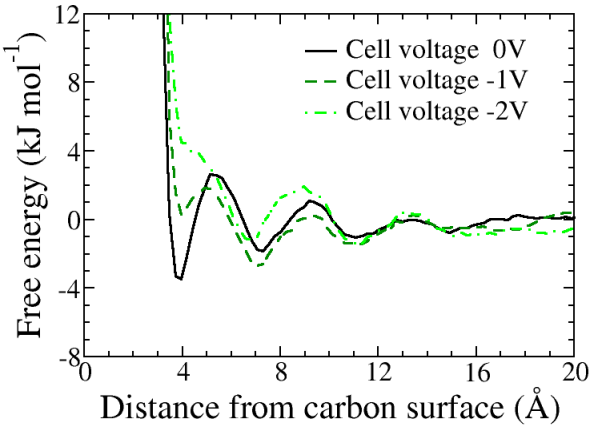

Figure S1: Free energy profiles for BF_4^- anions at negative potentials.

is clearly visible. Figure S2 shows the free energy profiles and integrated ion densities for BF_4^- in [BMI][BF_4]-ACN and [PEt_4][BF_4]-ACN at 0 V. The coarse-grained approach, used for [BMI][BF_4]-ACN, leads to stronger features compared to the all atom approach, used for [PEt_4][BF_4]-ACN. The density plots predict that more ions enter small pores (pore width $<$ 10 Å) in the case of [BMI][BF_4]-ACN compared to the case of [PEt_4][BF_4]-ACN.

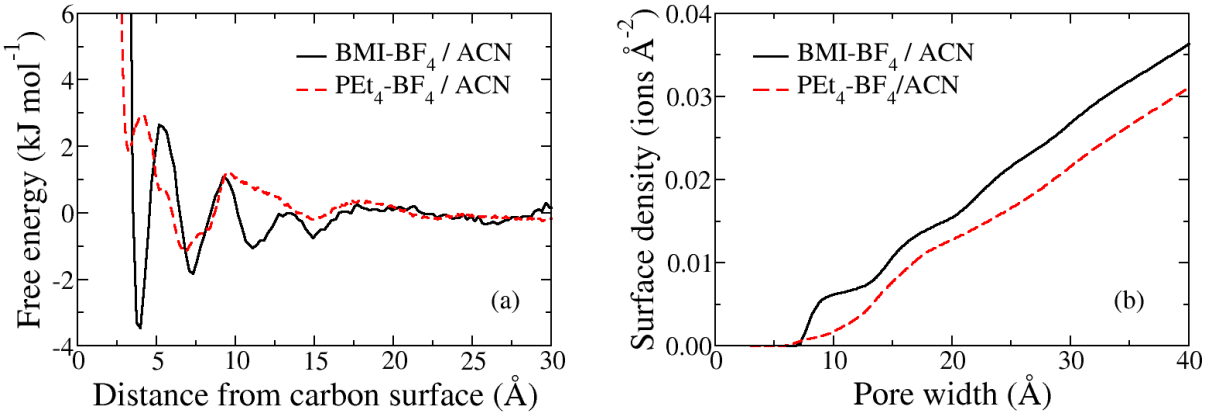

Figure S2: Free energy profiles (a) and integrated densities (b) of BF_4^- in [BMI][BF_4]-ACN (coarse-grained representation of the ions) and [PEt_4][BF_4]-ACN (all-atom representation of the ions) at 0 V.

3 Details of NICS calculations and intrapolation

DFT calculations are carried out on three simple aromatic hydrocarbons (coronene, circumcoronene, dicircumcoronene - see Figure S3), either neutral or with a charge of ± 1e, using Gaussian 09[S13]. Following earlier works,[S14–S16] a 6-31G(d) basis set and the B3LYP

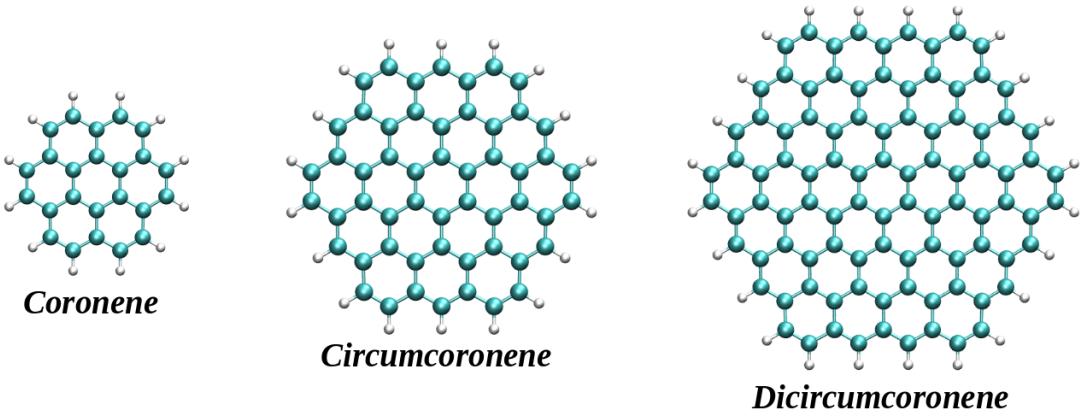

Figure S3: Aromatic molecules used for the NICS calculations.

exchange-correlation functional are used[S17]. After optimizing the structures, the NICS are calculated on a line going through the center of the molecule and perpendicular to its plane. The NICS are the isotropic shifts calculated by averaging over the diagonal components of

the shielding tensor:

$$\text{NICS} = -\frac{1}{3}\left(\sigma_{xx} + \sigma_{yy} + \sigma_{zz}\right) \tag{1}$$

where $\sigma_{\alpha\alpha}$ are the diagonal elements of the NICS tensor. Since the addition/removal of an electron on the molecule might lead to different convergence with basis set size compared to previous works on neutral molecules,[S14–S16] calculations with different basis sets were done on the coronene molecule. As shown in Figure S4, increasing the basis set beyond 6-31G(d)

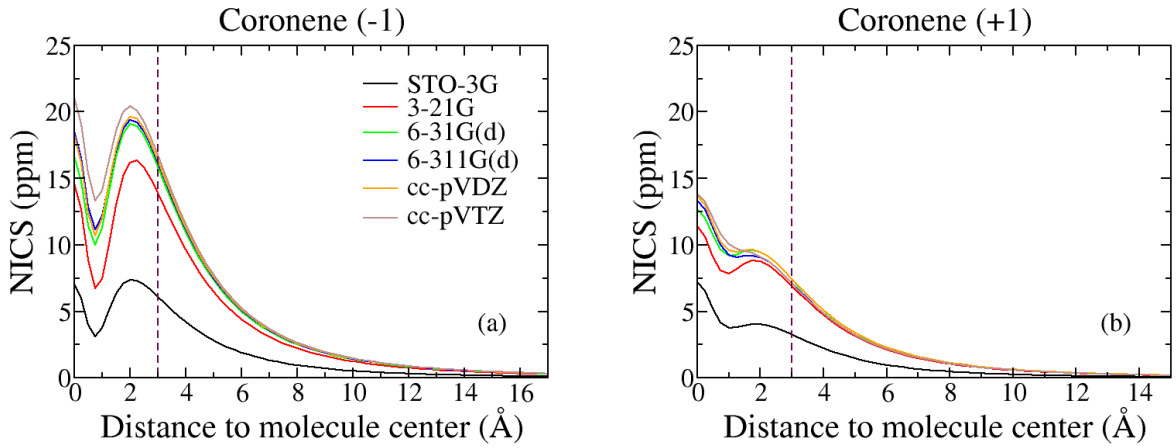

Figure S4: NICS calculated on a line going through the center of the molecule considered and perpendicular to its plane for negatively (a) and positively (b) charged coronene. Increasing the basis set beyond 6-31G(d) leads to negligible changes for distances larger than 3 Å, which are the ones relevant for ion adsorption.

leads to negligible changes for distances larger than 3 Å, which are the ones relevant for ion adsorption. The NICS calculated for the three coronenes considered here are shown in Figure S5. An interesting point to note is that there is a molecular size effect, i.e. the larger the molecule the larger the NICS, as was observed for neutral molecules in previous works.[S15,S18]

As described in the main text, the surface charges corresponding to the molecules used in this work carrying a full charge of ±1e are too large for the studied potential: 44.20 μC cm^{-2} for coronene, 16.31 μC cm^{-2} for circumcoronene and 8.37 μC cm^{-2} for dicircumcoronene. To obtain the NICS profiles for realistic surface charges, an intrapolation between the NICS for the neutral molecules and the NICS for the charged molecules is done. The surface charges

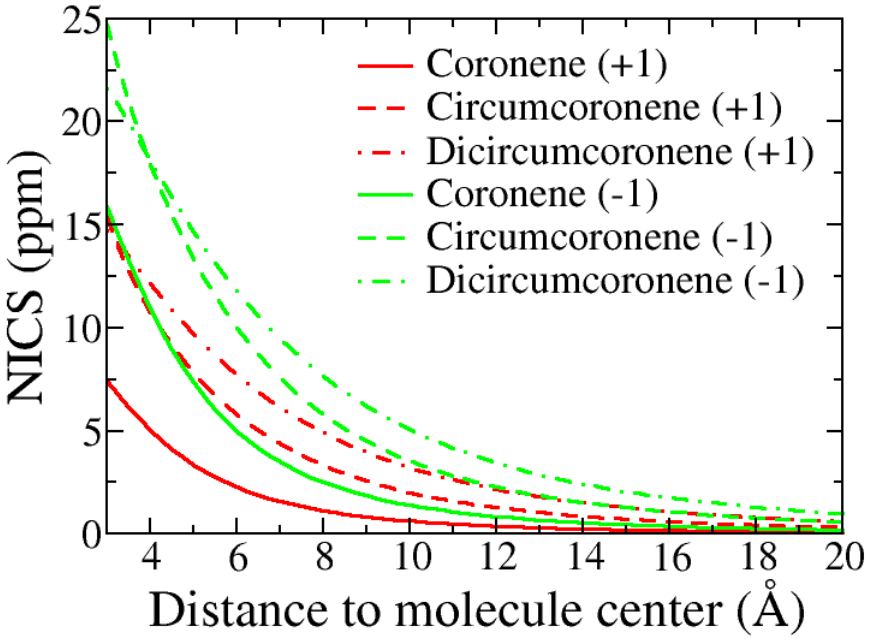

Figure S5: NICS calculated on a line going through the center of the molecule considered and perpendicular to its plane for negatively and positively charged coronenes studied in this work. Only distances larger than 3 Å are shown as these distances are the ones relevant for ion adsorption.

used for this intrapolation are given in Table S2.

Table S2: Surface charges used in the calculation of the NICS profiles at various potentials extracted from molecular simulations of [BMI][BF_4]-ACN in contact with planar electrodes.[S1] In that work, the surface charge was shown to vary only weakly with the electrolyte nature.

Cell voltage	0.5V	1.0V	1.5V	2V
Surface charge (μC cm^{-2})	± 1.33	± 2.43	± 3.82	± 4.89

4 Pore width and pore surface distribution

In this study, following previous works,[S19–S21] an arbitrarily chosen log normal distribution centred around the area of circumcoronene is used to determine the pore surfaces assigned to the lattice sites. To determine the pore widths, the pore size distribution obtained experimentally for YP50F is used.[S22]

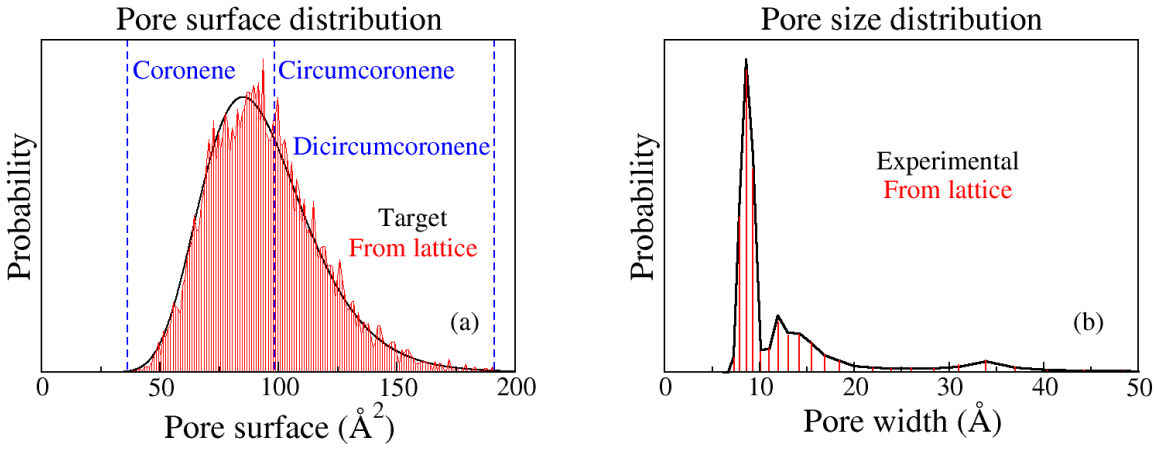

Figure S6: Pore surface (a) and pore size (b) distributions used to define the pore surface and width in the particle model.

As a consequence of the size effect seen for the NICS, the molecule used to define the pore surface of the slit pores in the particle model has an impact on the shift observed. Figure S7 shows the chemical shift at various potentials while using coronene, circumcoronene, dicircumcoronene or a distribution of areas centred on the area of circumcoronene to define the pore surface. It is noteworthy that the use of circumcoronene only or a distribution around its area does not affect the results significantly. On the contrary, the use of other molecules lead to large variations in both the shift values and the slope of the variation with potential. Interestingly, as can be seen in the main text, circumcoronene gives a good agreement for both the values and slopes. Nevertheless, this molecule will not necessarily be the best option for other porous carbons.[S18]

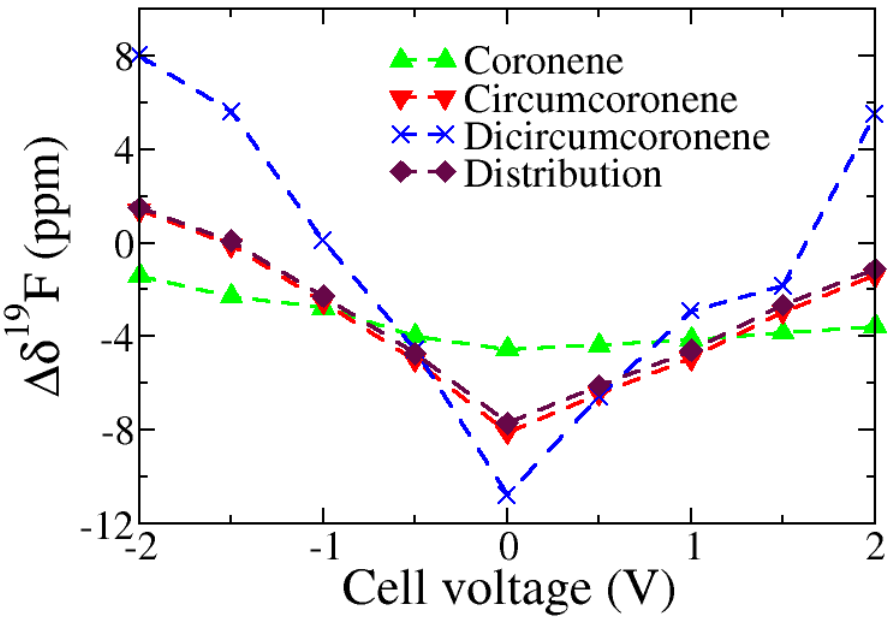

Figure S7: Chemical shifts simulated through the particle model for [BMI][BF_4]-ACN at various potentials for different molecules used to define pore surfaces.

5 Adsorption of PEt_4^+ and BF_4^- in small pores

Molecular dynamics simulations were conducted to assess how many PEt_4^+ cations and BF_4^- anions adsorb in a carbon with an average pore size of 8.6 Å, i.e. very close to the most common pore size of the YP-50F carbon of 8.5 Å. For this study, a relatively ordered carbon with a very well defined pore size was chosen, more precisely a GAP carbon reported in the study of Deringer *et al.*[S23] NPT and NVT simulations were done, using LAMMPS,[S10] on a system consisting in 130 ion pairs and 1,200 ACN molecules in contact with the GAP carbon (5,292 atoms). The NPT simulation was run until the volume of the simulation box was equilibrated and subsequent short NVT were done to estimate the number of ions adsorbed in the pores. The number of adsorbed ions is the number of ions with a center of mass having a z coordinate between z_{min} and z_{max}, the z coordinates of the two outer most carbons atoms.

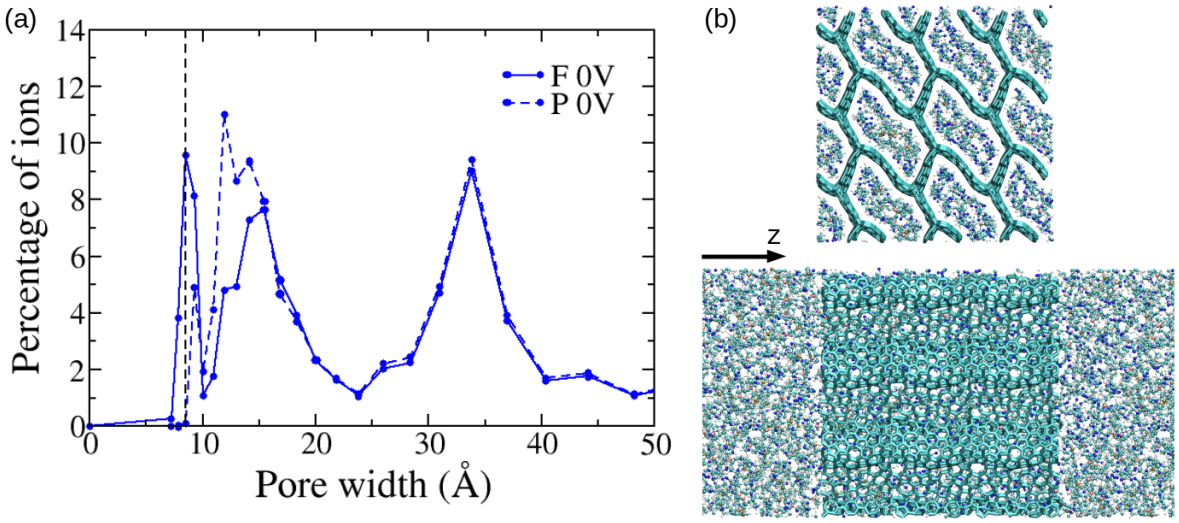

Figure S8: (a) Relative populations of ions in the pores obtained with the carbon particle model for $[PEt_4][BF_4]$-ACN at 0V. (b) Snapshot of molecular simulations conducted to determine the adsorption of ions in a porous carbon with an average pore size equal to 8.5 Å.

References

(S1) Merlet, C.; Salanne, M.; Rotenberg, B.; Madden, P. Influence of solvation on the structural and capacitive properties of electrical double layer capacitors. *Electrochim. Acta* **2013**, *101*, 262.

(S2) Canongia Lopes, J. N.; Deschamps, J.; Pádua, A. A. H. Modeling ionic liquids using a systematic all-atom force field. *J. Phys. Chem. B* **2004**, *108*, 2038–2047.

(S3) Canongia Lopes, J. N.; Pádua, A. A. H. Molecular force field for ionic liquids composed of triflate or bistriflylimide anions. *J. Phys. Chem. B* **2004**, *108*, 16893–16898.

(S4) Canongia Lopes, J. N.; Pádua, A. A. H. Molecular force field for ionic liquids III: Imidazolium, pyridinium, and phosphonium cations; chloride, bromide, and dicyanamide anions. *J. Phys. Chem. B* **2006**, *110*, 19586–19592.

(S5) Price, M. L. P.; Ostrovsky, D.; Jorgensen, W. L. Gas-phase and liquid-state properties of esters, nitriles, and nitro compounds with the OPLS-AA force field. *J. Comput. Chem.* **2001**, *22*, 1340–1352.

(S6) Cole, M. W.; Klein, J. R. The interaction between noble gases and the basal plane surface of graphite. *Surf. Sci.* **1983**, *124*, 547 – 554.

(S7) Siepmann, J. I.; Sprik, M. Influence of surface topology and electrostatic potential on water/electrode systems. *J. Chem. Phys.* **1995**, *102*, 511–524.

(S8) Pounds, M.; Tazi, S.; Salanne, M.; Madden, P. A. Ion adsorption at a metallic electrode: An *ab initio* based simulation study. *J. Phys.: Condens. Matter* **2009**, *21*, 424109.

(S9) Wang, Z.; Yang, Y.; Olmsted, D. L.; Asta, M.; Laird, B. B. Evaluation of the constant potential method in simulating electric double-layer capacitors. *J. Chem. Phys.* **2014**, *141*, 184102.

(S10) Plimpton, S. Fast parallel algorithms for short-range molecular dynamics. *J. Comp. Phys.* **1995**, *117*, 1–19.

(S11) Marin-Laflèche, A.; Haefele, M.; Scalfi, L.; Coretti, A.; Dufils, T.; Jeanmairet, G.; Reed, S. K.; Serva, A.; Berthin, R.; Bacon, C.; Bonella, S.; Rotenberg, B.; Madden, P. A.; Salanne, M. MetalWalls: A classical molecular dynamics softwarededicated to the simulation of electrochemical systems. *J. Open Source Softw* **2020**, *5*, 2373.

(S12) Pádua, A. A. H. fftool. `http://doi.org/10.5281/zenodo.18618`.

(S13) Frisch, M. J.; Trucks, G. W.; Schlegel, H. B.; Scuseria, G. E.; Robb, M. A.; Cheeseman, J. R.; Scalmani, G.; Barone, V.; Mennucci, B.; Petersson, G. A., et al. Gaussian 09, Revision D. 01, 2013, Gaussian. *Inc., Wallingford CT* **2013**,

(S14) Moran, D.; Stahl, F.; Bettinger, H. F.; Schaefer, H. F.; Schleyer, P. v. R. Towards graphite: Magnetic properties of large polybenzenoid hydrocarbons. *J. Am. Chem. Soc.* **2003**, *125*, 6746–6752.

(S15) Forse, A. C.; Griffin, J. M.; Presser, V.; Gogotsi, Y.; Grey, C. P. Ring current effects: Factors Affecting the NMR chemical shift of molecules adsorbed on porous carbons. *J. Phys. Chem. C* **2014**, *118*, 7508–7514.

(S16) Kilymis, D.; Bartók, A. P.; Pickard, C. J.; Forse, A. C.; Merlet, C. Efficient prediction of nucleus independent chemical shifts for polycyclic aromatic hydrocarbons. *Phys. Chem. Chem. Phys.* **2020**, *22*, 13746–13755.

(S17) Becke, A. D. Density-functional thermochemistry. III. The role of exact exchange. *J. Chem. Phys.* **1993**, *98*, 5648–5652.

(S18) Forse, A. C.; Merlet, C.; Allan, P. K.; Humphreys, E. K.; Griffin, J. M.; Aslan, M.; Zeiger, M.; Presser, V.; Gogotsi, Y.; Grey, C. P. New insights into the structure

of nanoporous carbons from NMR, Raman, and pair distribution function Analysis. *Chem. Mater.* **2015**, *27*, 6848–6857.

(S19) Merlet, C.; Forse, A. C.; Griffin, J. M.; Frenkel, D.; Grey, C. P. Lattice simulation method to model diffusion and NMR spectra in porous materials. *J. Chem. Phys.* **2015**, *142*, 094701.

(S20) Xing, Y.-Z.; Luo, Z.-X.; K., A.; Wu, Y. Probing carbon micropore size distribution by nucleus independent chemical shift. *Carbon* **2014**, *77*, 1132–1139.

(S21) Cervini, L.; Lynes, O. D.; Akien, G. R.; Kerridge, A.; Barrow, N. S.; Griffin, J. M. Factors affecting the nucleus-independent chemical shift in NMR studies of microporous carbon electrode materials. *Energy Storage Mater.* **2019**, *21*, 335–346.

(S22) Forse, A. C.; Griffin, J. M.; Merlet, C.; Carreteo-Gonzalez, J.; Raji, A.-R. O.; Trease, N. M.; Grey, C. P. Direct observation of ion dynamics in supercapacitor electrodes using *in situ* diffusion NMR spectroscopy. *Nature Energy* **2017**, *2*, 16216.

(S23) Deringer, V. L.; Merlet, C.; Hu, Y.; Lee, T. H.; Kattirtzi, J. A.; Pecher, O.; Csányi, G.; Elliott, S. R.; Grey, C. P. Towards an atomistic understanding of disordered carbon electrode materials. *Chem. Commun.* **2018**, *54*, 5988–5991.